Hindawi
Science and Technology of Nuclear Installations
Volume 2022, Article ID 5890896, 17 pages
https://doi.org/10.1155/2022/5890896

*Research Article*

# Multiple Assessments on the Gamma-Ray Protection Properties of Niobium-Doped Borotellurite Glasses: A Wide Range Investigation Using Monte Carlo Simulations

**H. O. Tekin,[1,2] Fatema T. Ali,[3] Ghada Almisned,[4] Gulfem Susoy,[5] Shams A. M. Issa,[6,7] Antoaneta Ene,[8] Wiam Elshami,[1] and Hesham M. H. Zakaly[7,9]**

[1]*Medical Diagnostic Imaging Department, College of Health Sciences, University of Sharjah, Sharjah 27272, UAE*
[2]*Istinye University, Faculty of Engineering and Natural Sciences, Computer Engineering Department, Istanbul 34396, Turkey*
[3]*Center for Advanced Materials Research, Research Institute of Sciences and Engineering, University of Sharjah, Sharjah 27272, UAE*
[4]*Department of Physics, College of Science, Princess Nourah Bint Abdulrahman University, P.O. Box 84428, Riyadh 11671, Saudi Arabia*
[5]*Department of Physics, Faculty of Science, Istanbul University, Istanbul 34134, Turkey*
[6]*Physics Department, Faculty of Science, University of Tabuk, Tabuk 71451, Saudi Arabia*
[7]*Physics Department, Faculty of Science, Al-Azhar University, Assiut 71524, Egypt*
[8]*INPOLDE Research Center, Department of Chemistry, Physics and Environment, Faculty of Sciences and Environment, Dunarea de Jos University of Galati, 47 Domneasca Street, Galati 800008, Romania*
[9]*Institute of Physics and Technology, Ural Federal University, Yekaterinburg 620002, Russia*

Correspondence should be addressed to Ghada Almisned; gaalmisned@pnu.edu.sa, Antoaneta Ene; antoaneta.ene@ugal.ro, and Hesham M. H. Zakaly; h.m.zakaly@azhar.edu.eg

Received 20 December 2021; Revised 14 February 2022; Accepted 19 February 2022; Published 18 March 2022

Academic Editor: Kai Xu



In this study, the monotonic effect of $Ta_2O_5$ and $ZrO_2$ in some selected borotellurite glasses was investigated in terms of their impact on gamma-ray-shielding competencies. Accordingly, three niobium-reinforced borotellurite glasses ($S1: 75TeO_2 + 15B_2O_3 + 10Nb_2O_5$, $S2: 75TeO_2 + 15B_2O_3 + 9Nb_2O_5 + 1Ta_2O_5$, and $S3: 75TeO_2 + 15B_2O_3 + 8Nb_2O_5 + 1Ta_2O_5 + 1ZrO_2$) were modelled in the general-purpose MCNPX Monte Carlo code. They have been defined as an attenuator sample between the point isotropic gamma-ray source and the detector in terms of determining their attenuation coefficients. To verify the MC results, attenuation coefficients were then compared with the Phy-X/PSD program data. Our findings clearly demonstrate that although some behavioral changes occurred in the shielding qualities, modest improvements occurred in the attenuation properties depending on the modifier variation and its magnitude. However, the replacement of 2% moles of $Nb_2O_5$ with 1% mole of $Ta_2O_5$ and 1% mole of $ZrO_2$ provided significant improvements in both glass density and attenuation properties against gamma rays. Finally, the HVL values of the S3 sample were compared with some glass- and concrete-shielding materials and the S3 sample was reported for its outstanding properties. As a consequence of this investigation, it can be concluded that the indicated type of additive to be added to borotellurite glasses will provide some advantages, particularly when used in radiation fields, by increasing the shielding qualities moderately.

## 1. Introduction

Radiation is being used in a number of different ways in medicine, including the generation of energy for diagnostic and therapeutic applications. Because radiation cannot be eliminated, protective steps should be taken to minimize its harmful effects. Traditionally, lead (Pb) has the highest atomic number among materials that have a wide usage area

Table 1: Code, chemical composition, elemental composition, and density ($\rho$) of the prepared glasses.

| Code | Chemical composition wt.% | | | | | Elemental composition wt.% | | | | | | $\rho$ (g/cm$^3$) |
|---|---|---|---|---|---|---|---|---|---|---|---|---|
| | $TeO_2$ | $B_2O_3$ | $Nb_2O_5$ | $Ta_2O_5$ | $ZrO_2$ | Te | O | B | Nb | Ta | Zr | |
| S1 | 0.764 | 0.067 | 0.170 | 0 | 0 | 0.6106 | 0.2501 | 0.0207 | 0.1186 | — | — | 4.88 |
| S2 | 0.755 | 0.066 | 0.151 | 0.028 | 0 | 0.6038 | 0.2473 | 0.0205 | 0.1055 | 0.0228 | — | 4.93 |
| S3 | 0.762 | 0.066 | 0.135 | 0.028 | 0.008 | 0.6093 | 0.2465 | 0.0207 | 0.0946 | 0.0230 | 0.0058 | 4.94 |

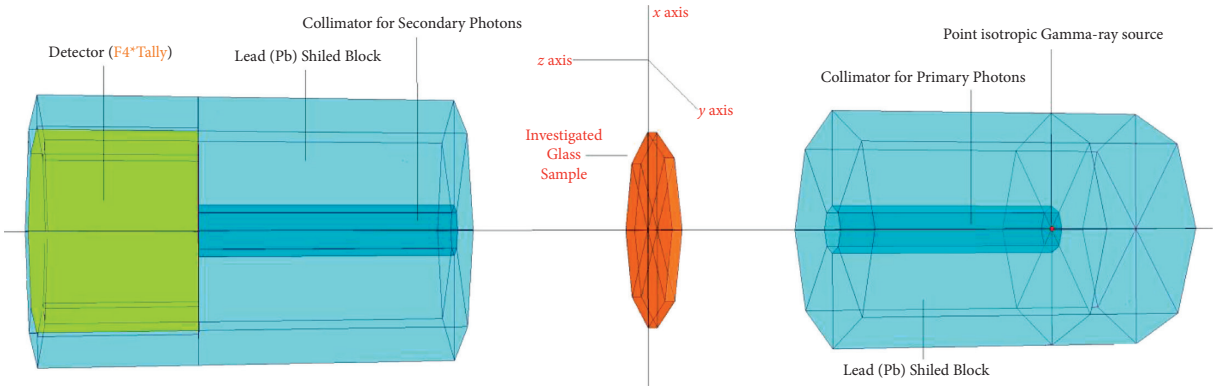


Figure 1: 3D view of the MCNPX simulation setup utilized for gamma-ray transmission simulations (obtained from the MCNPX visual editor visedX22S).

in the field of radiation shielding. On the other hand, concrete with low cost, easy use, and good structural properties can also be used as an excellent shielding material. The fact that concrete shielding is primarily utilized in construction is far and by the most important disadvantage, owing to its massive structure and weight. The development of novel glass materials for efficient radiation shielding presents numerous untapped research opportunities. Radiation protection material design is heavily reliant on understanding the interactions between radiation and the materials used to protect against it. Pb or products containing Pb have a number of disadvantages, the most significant of which being their toxicity and consequent risk to users and the environment as well as difficulties faced during the attenuation of low-energy X-ray photons [1–9]. As a result, there has been an increase in recent years in the consideration of lead-free glasses as gamma-ray-shielding materials. This is because many glass compositions have good radiation-shielding capacities and have unique properties such as optical transparency, compatibility for structural modifications as well as radiation absorption. Researchers have been developing various types of radiation-shielding glass for several decades, including borate-, silicate-, phosphate-, boro-silicate-, and tellurite-based glass. Indeed, the glass former has an impact on the overall characteristics of the glass matrix. Researchers have been particularly interested in the combination of borate and tellurite, one of many glass-based oxides, due to the distinct properties of these two oxides, such as low melting point, nontoxicity, high refractive index, low phonon energy, chemical and thermal stability, high density, transparency over a wide spectral range, and corrosion resistance [10–20]. Various studies on the gamma-ray-shielding properties of tellurite glasses have been conducted in the literature [21–29]. In their pure form, tellurite glasses can crystallize readily and are therefore unstable. Consequently, the addition of other network formers and modifiers, such as alkaline-earth metals, alkaline metals, and transition metal oxides, helps stabilize the system [30]. Transparency, thermal stability, and optical transmittance are all enhanced by $TeO_2$ glasses containing a significant amount of $B_2O_3$ [31]. In addition, using boron oxide is important in glass samples where the thermal expansion coefficient is desired to be low. On the other hand, it increases the resistance of the glass to chemical effects and gives it the ability to refract light. On the other hand, the fact that $Nb_2O_5$ and $Ta_2O_5$ have empty D-orbitals increases the nonlinear optical response [32–36]. Finally, the $ZrO_2$ modifier raises the thermal and chemical stability of glass while also increasing viscosity, melting temperature, and glass transition temperature [37–39]. Although several studies have shown the effect of glass-forming oxides and modifier oxides on the structure and properties of telluride glass, their radiation-shielding properties remain a subject of research. The literature review showed that no previous research has examined the impact of $Nb_2O_5$ on borotellurite glasses' absorption capacities using Monte Carlo simulations for gamma rays. Consequently, in this study, we present an analysis of the gamma-ray radiation protection properties of $Nb_2O_5$ added to borotellurite glass [40]. The nominal compositions of the investigated glass sample are shown below.]

(i) $75TeO_2+15B_2O_3+10Nb_2O_5$ ($\rho = 4.88$ g/cm$^3$)

(ii) $75TeO_2+15B_2O_3+9Nb_2O_5+1Ta_2O_5$ ($\rho = 4.93$ g/cm$^3$)

(iii) $75TeO_2+15B_2O_3+8Nb_2O_5+1Ta_2O_5+1ZrO_2$ ($\rho = 4.94$ g/cm$^3$)

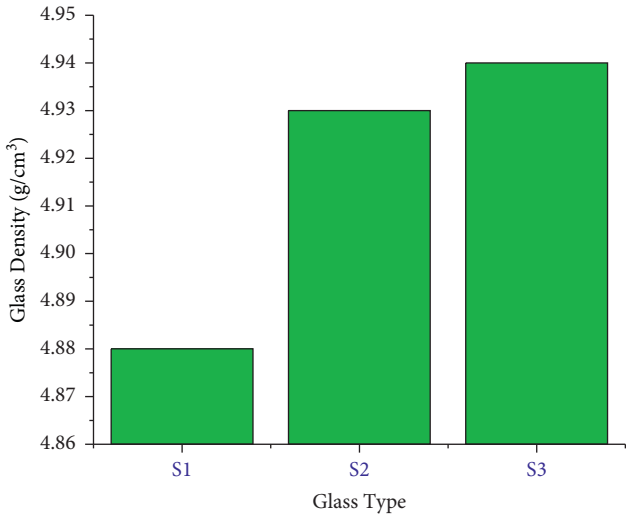


Figure 2: Variation of glass densities (g/cm$^3$).

Table 2: Comparison of the mass attenuation coefficients obtained from MCNPX and Phy-X/PSD.

| Energy (MeV) | S1 | | S2 | | S3 | |
|---|---|---|---|---|---|---|
| | MCNPX | Phy-X/PSD | MCNPX | Phy-X/PSD | MCNPX | Phy-X/PSD |
| 0.015 | 35.1255 | 34.6423 | 37.4591 | 37.0046 | 37.795 | 37.1618 |
| 0.02 | 23.9864 | 23.6582 | 24.0345 | 23.9379 | 24.1215 | 23.6609 |
| 0.03 | 8.1256 | 8.0697 | 8.1274 | 8.1670 | 8.1317 | 8.0690 |
| 0.04 | 14.1317 | 14.1262 | 14.2141 | 14.0600 | 14.2223 | 14.1082 |
| 0.05 | 7.8412 | 7.8360 | 7.8527 | 7.8016 | 7.8606 | 7.8291 |
| 0.06 | 4.8317 | 4.8281 | 4.8412 | 4.8087 | 4.8487 | 4.8258 |
| 0.08 | 2.2554 | 2.2522 | 2.3815 | 2.3787 | 2.3881 | 2.3879 |
| 0.10 | 1.2764 | 1.2642 | 1.3431 | 1.3363 | 1.3438 | 1.3413 |
| 0.15 | 0.4841 | 0.4809 | 0.5096 | 0.5058 | 0.5099 | 0.5074 |
| 0.20 | 0.2734 | 0.2704 | 0.2824 | 0.2820 | 0.2831 | 0.2828 |
| 0.30 | 0.1492 | 0.1474 | 0.1517 | 0.1514 | 0.1524 | 0.1516 |
| 0.40 | 0.1109 | 0.1091 | 0.1123 | 0.1110 | 0.1125 | 0.1111 |
| 0.50 | 0.0921 | 0.0909 | 0.0924 | 0.0920 | 0.0927 | 0.0920 |
| 0.60 | 0.0820 | 0.0800 | 0.0812 | 0.0807 | 0.0815 | 0.0807 |
| 0.80 | 0.0684 | 0.0669 | 0.0681 | 0.0672 | 0.0683 | 0.0672 |
| 1.00 | 0.0593 | 0.0587 | 0.0591 | 0.0589 | 0.0595 | 0.0589 |
| 1.50 | 0.0486 | 0.0472 | 0.0479 | 0.0472 | 0.0482 | 0.0472 |
| 2.00 | 0.0423 | 0.0414 | 0.0419 | 0.0415 | 0.0421 | 0.0415 |
| 3.00 | 0.0372 | 0.0361 | 0.0371 | 0.0362 | 0.0373 | 0.0362 |
| 4.00 | 0.0342 | 0.0338 | 0.0345 | 0.0340 | 0.0347 | 0.0340 |
| 5.00 | 0.0336 | 0.0329 | 0.0337 | 0.0330 | 0.0339 | 0.0330 |
| 6.00 | 0.0334 | 0.0325 | 0.0335 | 0.0327 | 0.0336 | 0.0327 |
| 8.00 | 0.0337 | 0.0327 | 0.0338 | 0.0330 | 0.0339 | 0.0330 |
| 10.00 | 0.0339 | 0.0335 | 0.0341 | 0.0337 | 0.0344 | 0.0338 |
| 15.00 | 0.0361 | 0.0359 | 0.0365 | 0.0362 | 0.0367 | 0.0362 |

Gamma radiation attenuation parameters like mass attenuation coefficients, effective atomic numbers, and half-value relay (HVL) were calculated using the MCNPX [41] simulation code and the Phy-X/PSD program [42] with varying photon energies in the current work. In subsequent sections of this paper, the technical aspects as well as the theoretical underpinnings of the current investigation will be discussed in detail. This work's findings may be useful for future uses of the glass types investigated for radiation shielding in nuclear reactors. In addition, the findings may be useful for a better understanding of borotellurite glasses in the gamma-ray-shielding applications.

## 2. Materials and Methods

*2.1. Glass Samples.* In this study, the nuclear radiation-shielding properties of $Ta_2O_5$- and $ZrO_2$-doped niobium-borotellurite glasses [40] were characterized in a wide energy

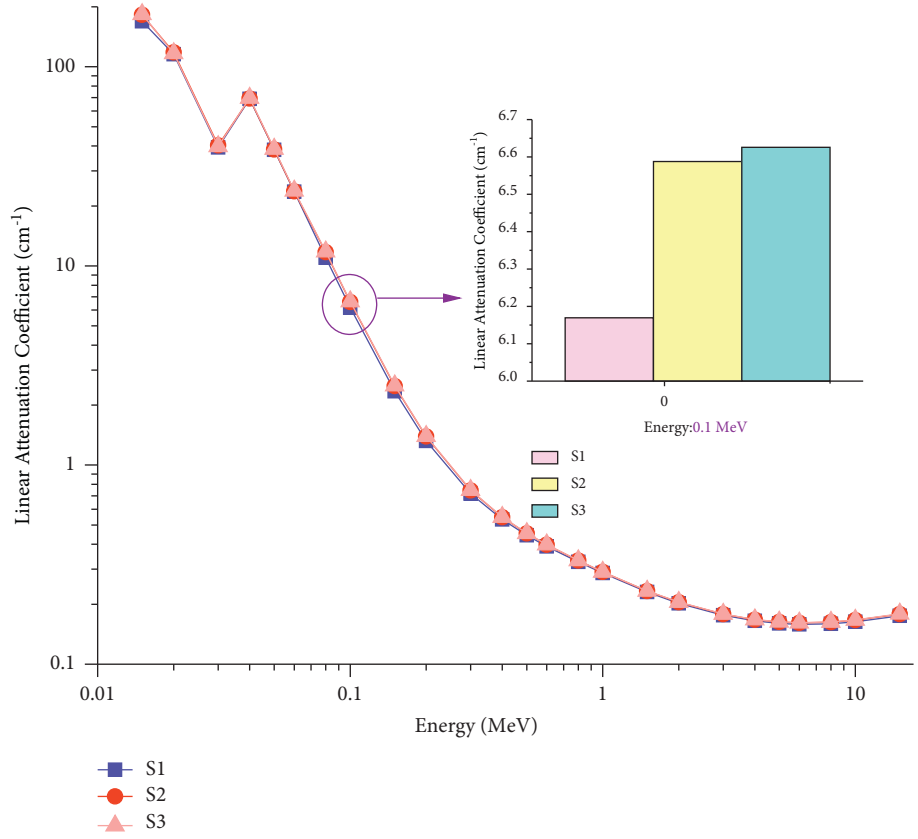


Figure 3: Variations of the linear attenuation coefficient ($cm^{-1}$) with photon energy (MeV) for all S1–S3 glasses.

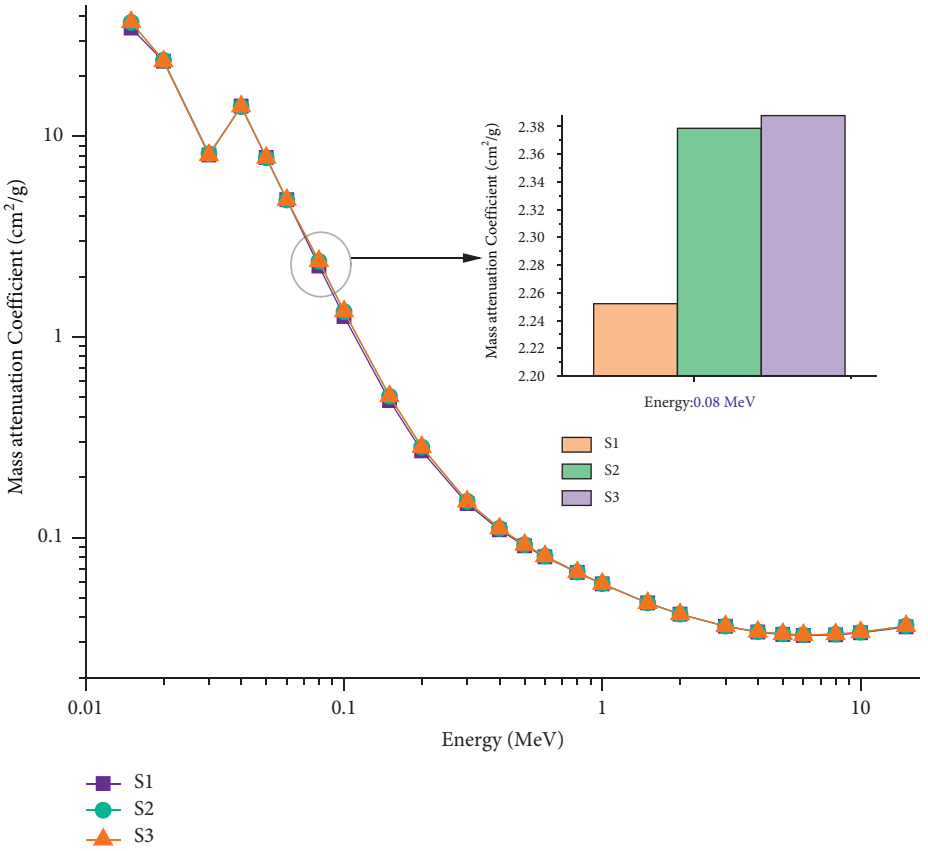


Figure 4: Variations of the mass attenuation coefficient ($cm^2/g$) with photon energy (MeV) for all S1–S3 glasses.

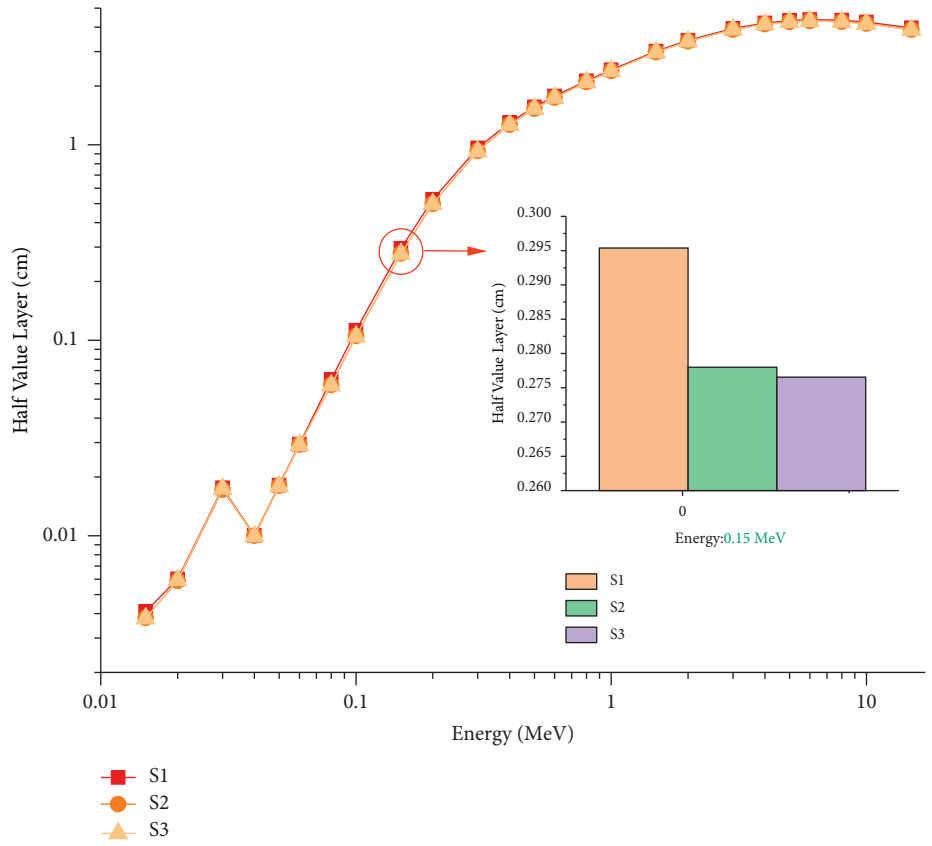


Figure 5: Variations of the half-value layer (cm) with photon energy (MeV) for all S1–S3 glasses.

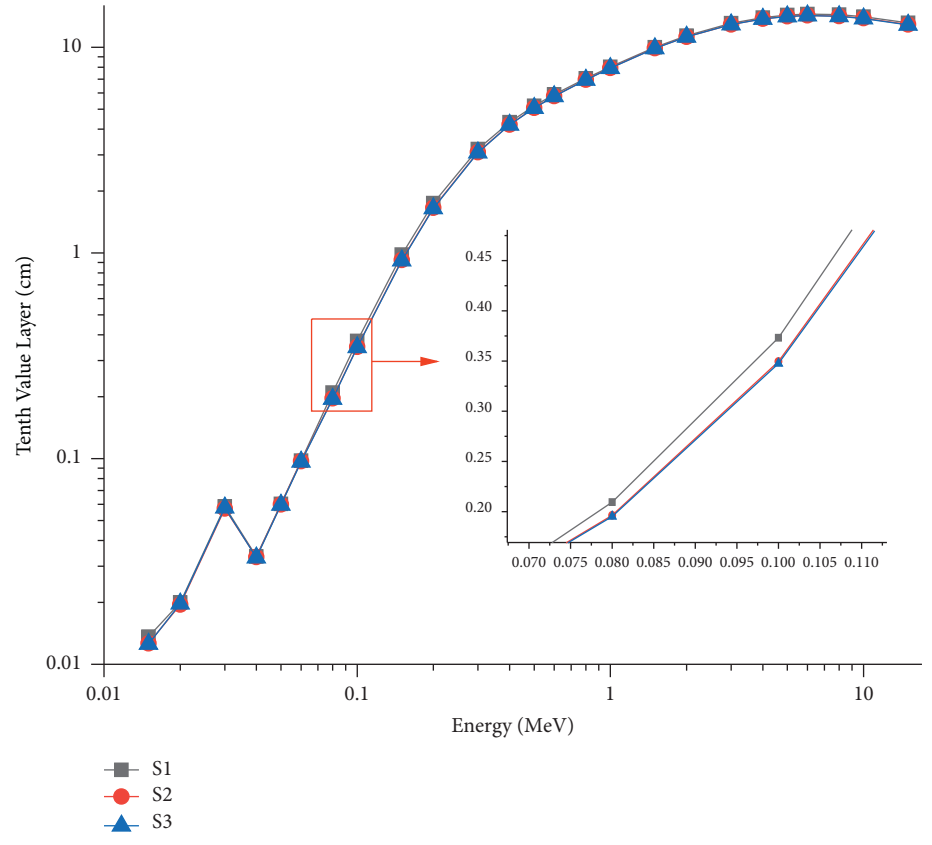


Figure 6: Variations of the tenth value layer (cm) with photon energy (MeV) for all S1–S3 glasses.

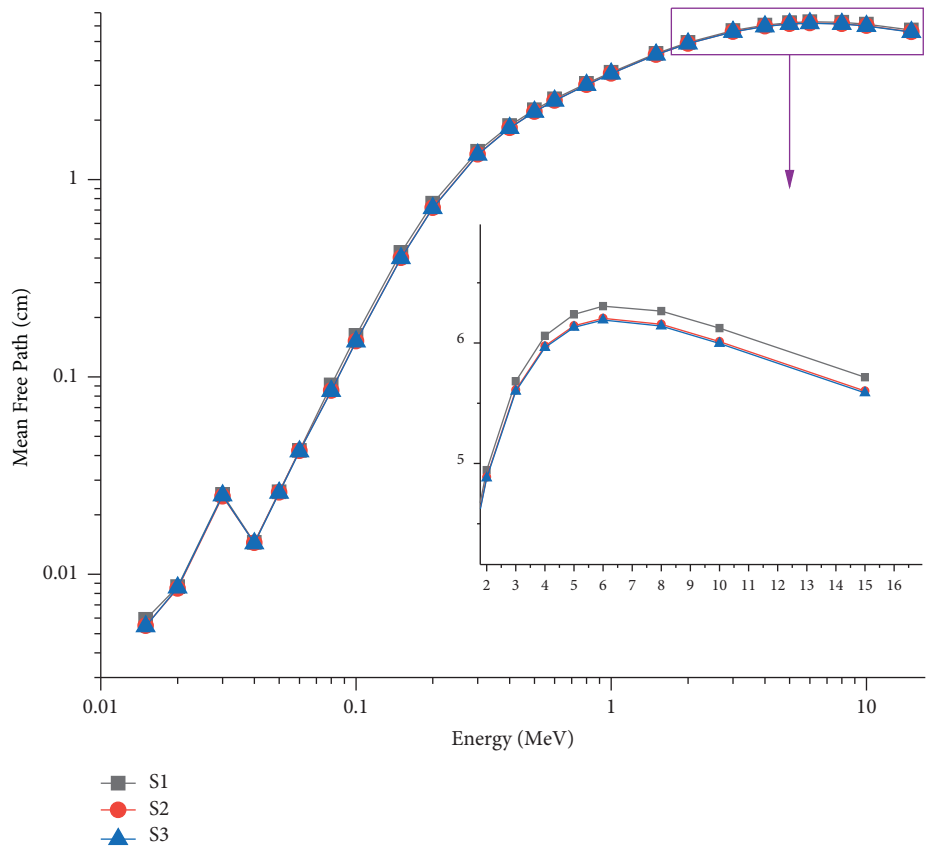


Figure 7: Variations of the mean free path (cm) with photon energy (MeV) for all S1–S3 glasses.

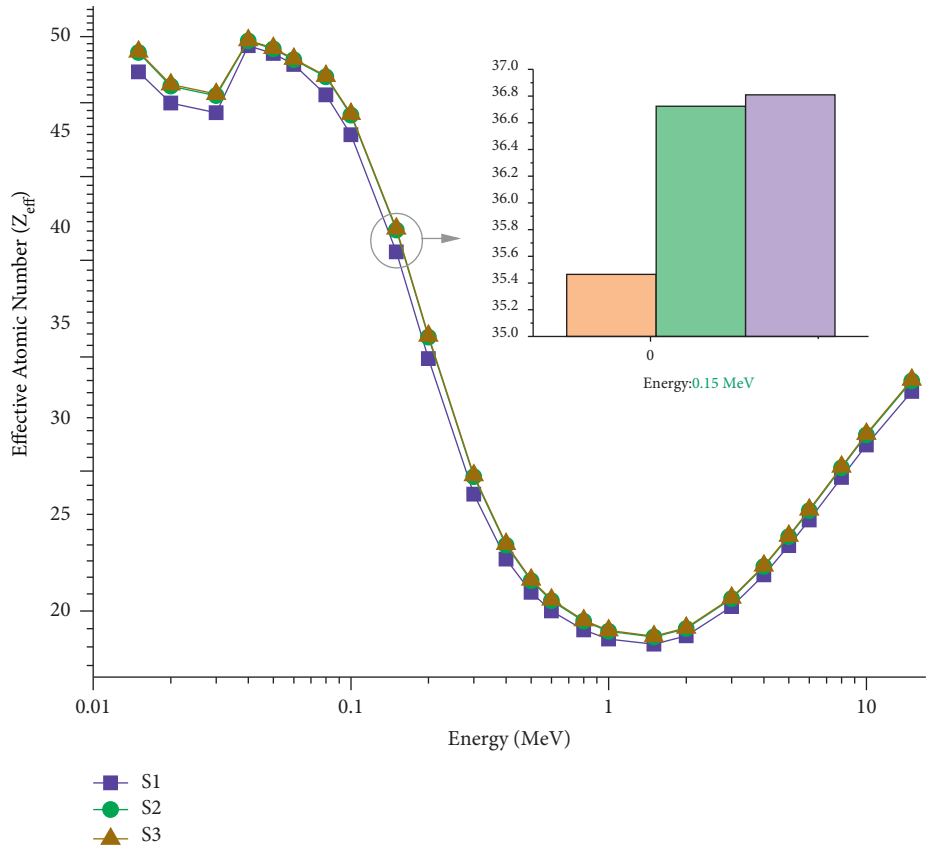


Figure 8: Variations of the effective atomic number ($Z_{eff}$) with photon energy (MeV) for all S1–S3 glasses.

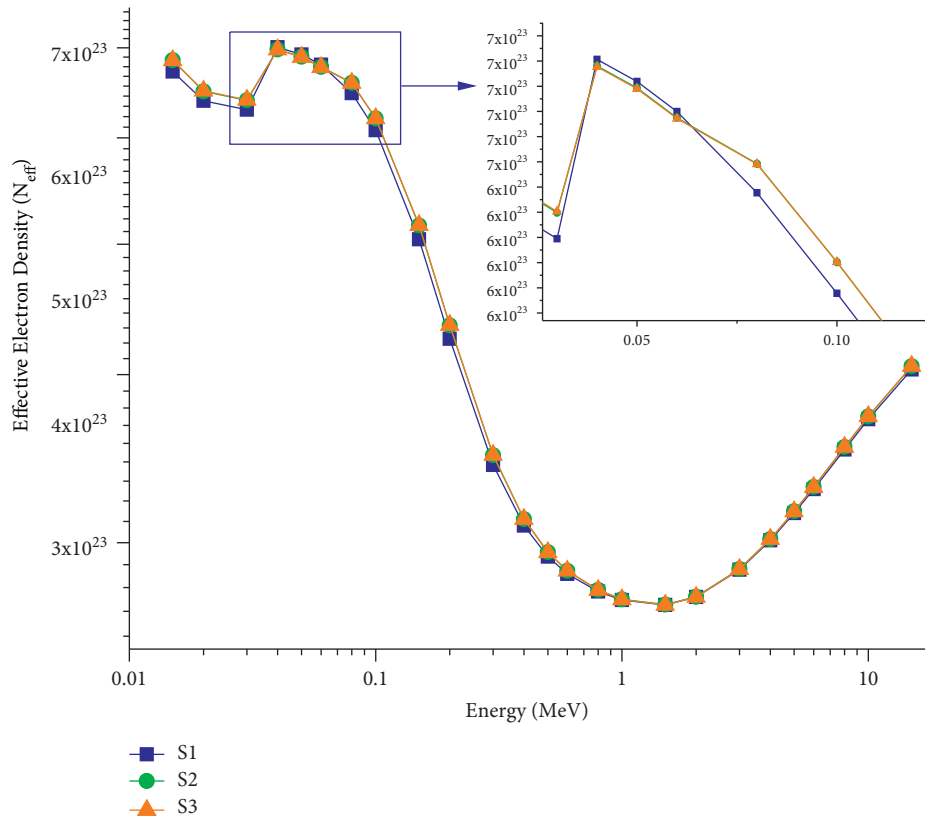


Figure 9: Variations of the effective electron density ($N_{eff}$) with photon energy (MeV) for all S1–S3 glasses.

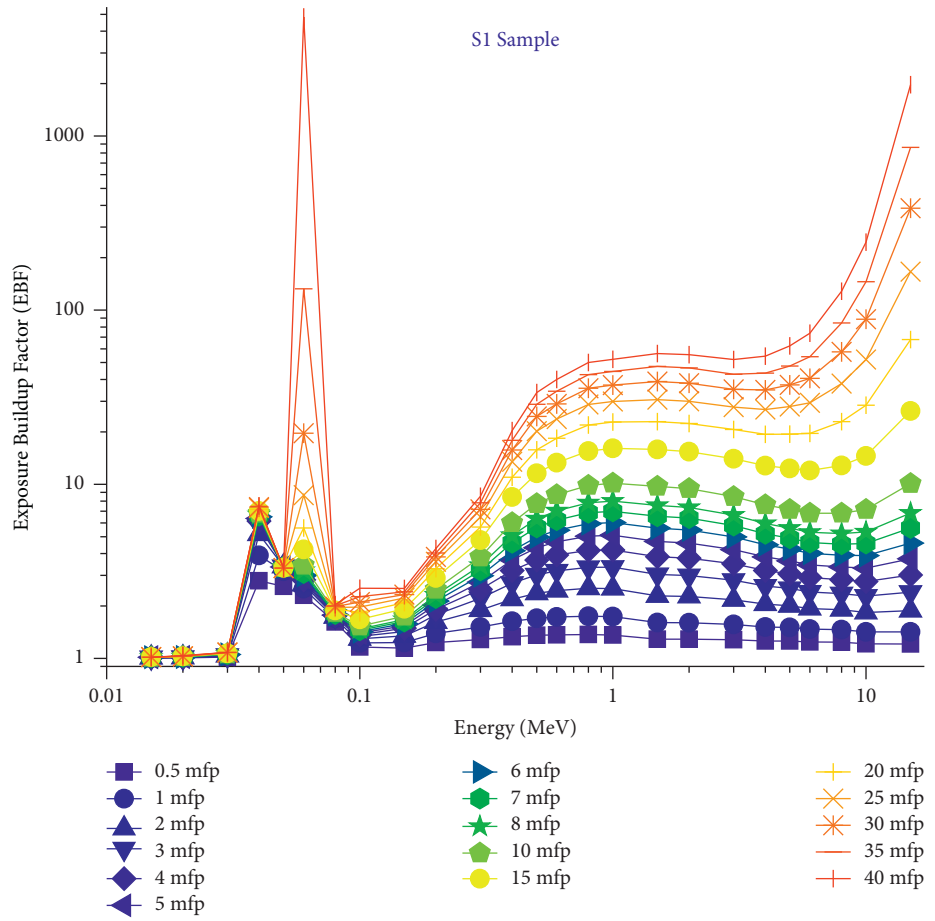


Figure 10: Demonstrates the relationship between the energy and EBF of the S1 sample.

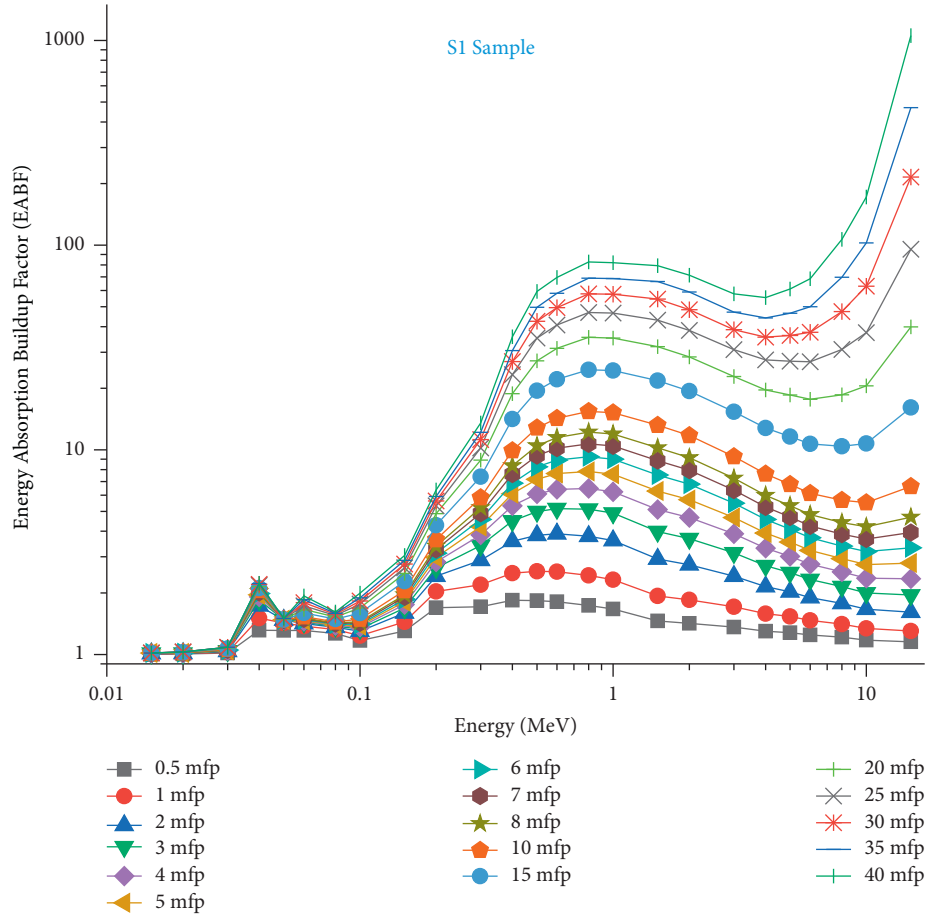


Figure 11: Demonstrates the relationship between the energy and EABF of the S1 sample.

range (i.e., from 0.015 MeV to 15 MeV). $Nb_2O_5$ was replaced with 1 mol % $Ta_2O_5$ and 1 mol % $ZrO_2$ to evaluate the influence of modifier oxides. As a result, we examined this substitution as a possible monotonic influence on the gamma-ray-shielding behaviors of the analyzed glasses, as well as the effect of the alterations on the gamma-ray-shielding characteristics.

*2.2. Determination of Gamma-Ray-Shielding Properties Using the MCNPX Monte Carlo Code.* The attenuation coefficients of the glasses under examination were calculated using MCNPX (Monte Carlo N-Particle eXtended) version 2.6.0. MCNPX is a fully three-dimensional (three-dimensional) general-purpose application that utilizes upgraded nuclear cross-section libraries and physics models. The shape of the entire gamma-ray transmission setup was modelled using the MCNPX code's INPUT file as a first step in the simulation technique. The INPUT file of MCNPX is composed of three major components: a CELL card, a SURFACE card, and a DATA card. To start, we determined the CELL structures of the simulation equipment by defining their covering surfaces and densities. Additionally, the CELL card component has been defined for each glass sample considering their elemental compositions, which are already described in the material IDs (Mn) section taking into account their elemental mass fractions (see Table 1). Following that, the geometrical alignments of the surfaces for the glass attenuator material, as well as the geometrical structures of the surfaces, which may be planar, spherical, or cone, were entered. We included the radioisotope energies (from 0.015 MeV to 15 MeV, respectively) as well as the source geometry as point isotropic to the DATA card area. Figure 1 depicts the overall geometry of the successfully designed simulation setup. Additionally, we added a critical specification to the DATA card for the data gathering mechanism, which is stated as TALLY MESH. The outcome function of the modelled gamma-ray transmission setup was constructed in this work utilizing the MCNPX`s F4 TALLY MESH. F4 tally is used to record the average flux in a point. Thereafter, attenuation coefficients of the glasses under investigation were determined using the well-known equation, namely the Beer–Lambert law.

$$I = I_0 e^{-\mu t}, \tag{1}$$

where $\mu$ ($cm^{-1}$) is the linear attenuation coefficient of the sample and $t$ is the physical thickness (cm) of the shielding material. To understand gamma energy loss as it passes through the shielding material, the mass attenuation coefficients ($\mu/\rho$) can be used for the shielding materials [40]. The mass attenuation coefficient of a compound or mixture is

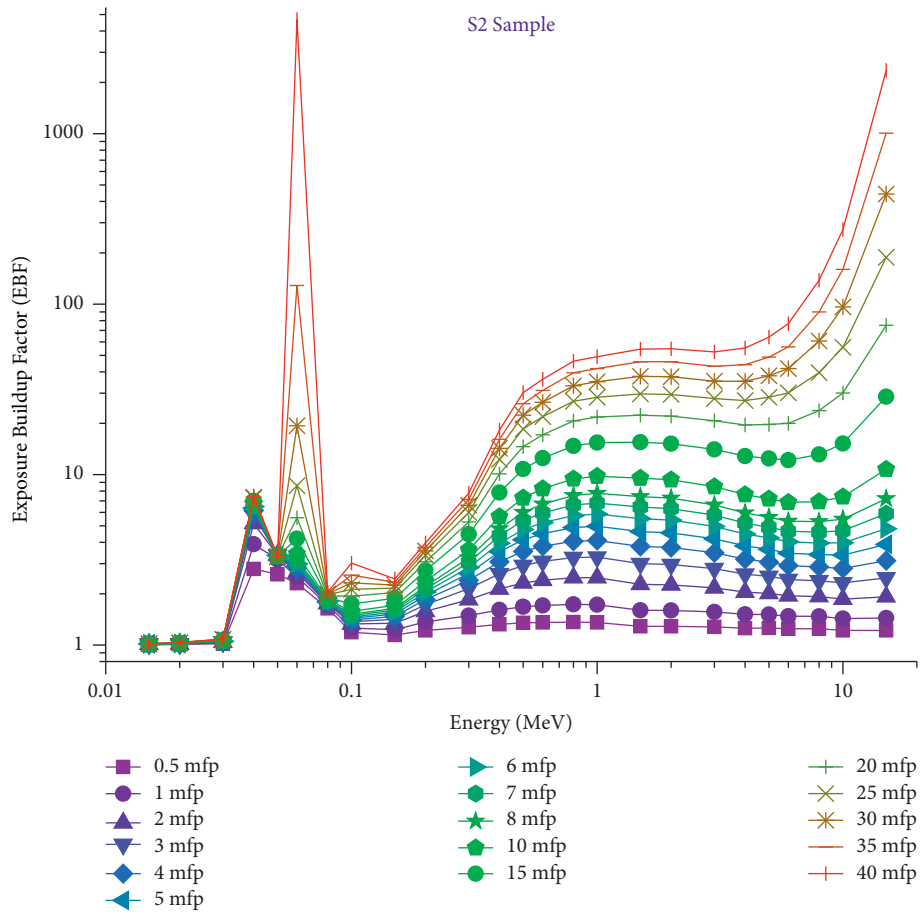


Figure 12: Demonstrates the relationship between the energy and EBF of the S2 sample.

calculated by summing the individual contributions of each of the elements that make up the mixture or compound (see for detailed calculation [43–45]. The obtained attenuation coefficients are then used for other critical shielding parameters, namely the tenth value layer (TVL), the half-value layer (HVL), and the mean free path (MFP).

## 3. Results and Discussions

The influence of $Ta_2O_5$ and $ZrO_2$ on the gamma-ray attenuation capacities of three niobium-doped borotellurite glasses was examined in this work. The aim of the current investigation was to investigate the monotonic effect of varying molar contributions of $Ta_2O_5$ and % $ZrO_2$ on niobium-doped borotellurite glass. It's well known that the material density has a great impact on the shielding properties of the materials. Comparing the three glass samples' densities showed that the S3 sample had the highest density value at 4.94 g/cm$^3$ followed by S2 at 4.93 g/cm$^3$, and then the S1 sample marking the lowest density at 4.88 g/cm$^3$ (see Figure 2). The variances between the glasses were not as high due to their comparable chemical compositions and a small number of molar changes across the replacements. However, it is seen that the replacement of 2% moles $Nb_2O_3$ with 1% mole $Ta_2O_5$+ 1% mole $ZrO_2$ caused an increment in the glass density as 0.06 g/cm$^3$. Along with the elemental alterations and their effect on gamma-ray-shielding behaviors, the given findings may be interpreted in terms of the 0.06 g/cm$^3$ density difference between the S1, S2, and S3 samples. Calculations for the overall study were conducted in two distinct phases. In the first phase, we utilized the MCNPX algorithm to determine the attenuation coefficients of the glass samples under investigation. To validate our findings, we compared them to those obtained using the Phy-X/PSD tool (see Table 2). Finally, since we verified two approaches, we utilized the Phy-X/PSD code to retrieve the remaining critical values. Figures 3 and 4 depict the numerical variations of the linear ($\mu$) and mass ($\mu_m$)attenuation coefficients of the glasses. As it is seen, both figures share almost identical trends that exhibit a sharp decrease followed by a sharp increase in mass and linear attenuation coefficients at 0.03 and 0.04 MeV energies with gradual decreasing afterwards. The sharp changes in the linear and mass attenuation coefficients of the glasses can be explained by the photon–matter interactions in different energy zones such as low, middle and high energy, where the photoelectric effect, Compton scattering, and pair production are dominant, respectively [46–48]. It is seen that the variations share almost the same pattern of difference among the S1, S2, and S3 glass types, which is demonstrated in the zoomed-in graphs. As mentioned before, the linear attenuation of a material is density dependent, while the mass attenuation

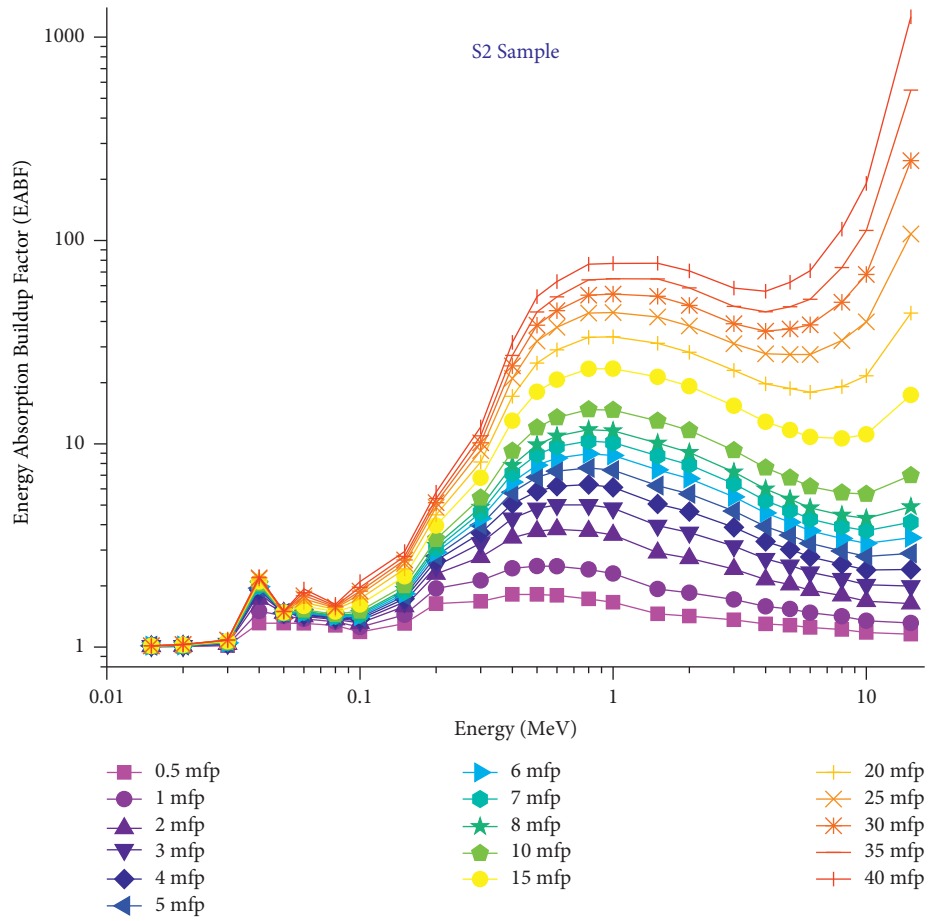


Figure 13: Demonstrates the relationship between the energy and EABF of the S2 sample.

coefficient is not. As it is seen from Figure 3, there are slight variations between the linear attenuation coefficients of the three glasses. This situation can be explained by similar density values of the glasses under investigation [49, 50]. However, the similarity in the linear and mass attenuation coefficients (see Figure 4) among the three glasses may also be attributed to the similarities in the elemental compositions of the S1, S2, and S3 glasses since replacements have been used with 1% molar differences between the above-mentioned structures. However, our findings showed that the S3 sample has the highest linear and mass attenuation coefficients at all the gamma-ray energies studied. Calculating the half-value layer (HVL) of a shielding material is a critical way for determining its effectiveness against the radiation being employed [51, 52]. The half-value layer (HVL) is the thickness of a material required to reduce the air-kerma intensity of an X-ray or gamma-ray to half of its initial value. Variations of the half-value layer (cm) with photon energy (MeV) for all S1–S3 glasses are demonstrated in Figure 5. The variation trend of the reported HVL values starts with a gradual increase until 0.03 MeV, where a sharp decrease occurs which results in 0.010 cm value for all glasses; then, it returns to the same pattern of gradual increase in values. At 0.015 MeV, a zoom-in column graph clearly shows the difference among the glasses. Our finding revealed that the S3 sample has the minimum half-value layer thickness at all gamma-ray energies. One may conclude that the minimum material thickness necessary to halve the same amount of gamma-ray energy between the three glasses is the S3 sample, due to its better attenuation capabilities. Similar to the term high value layer (HVL), the tenth value layer (TVL) refers to a certain thickness value for a material necessary to reduce the initial gamma-ray intensity by one-tenth (1/10). Our findings showed that the tenth value layer (cm) graph (See Figure 6) exhibits the same trend behavior and the same difference among the glasses, where the S2 and S3 values are closer to each other, giving S3 the lowest rank in values and S1 the highest. One may conclude that the S3 sample is preferable not just for the HVL values but also for the TVL values in terms of lowering the initial gamma-ray intensity at the smallest material thicknesses. The term mean free path is very helpful in assessing the mean distance between two consecutive gamma-ray interactions in the attenuator material. Figure 7 describes the relationship of the mean free path variations (cm) with photon energy (MeV) for all S1–S3 glasses, which also demonstrates a very similar trend behavior to the HVL and TVL graphs, giving S1 the highest values followed by S2 and S3. As a result, the mean distance between two consecutive interactions in the S3 sample is the lowest among the glasses under consideration, due to its superiority in terms of the interaction frequency with the incoming

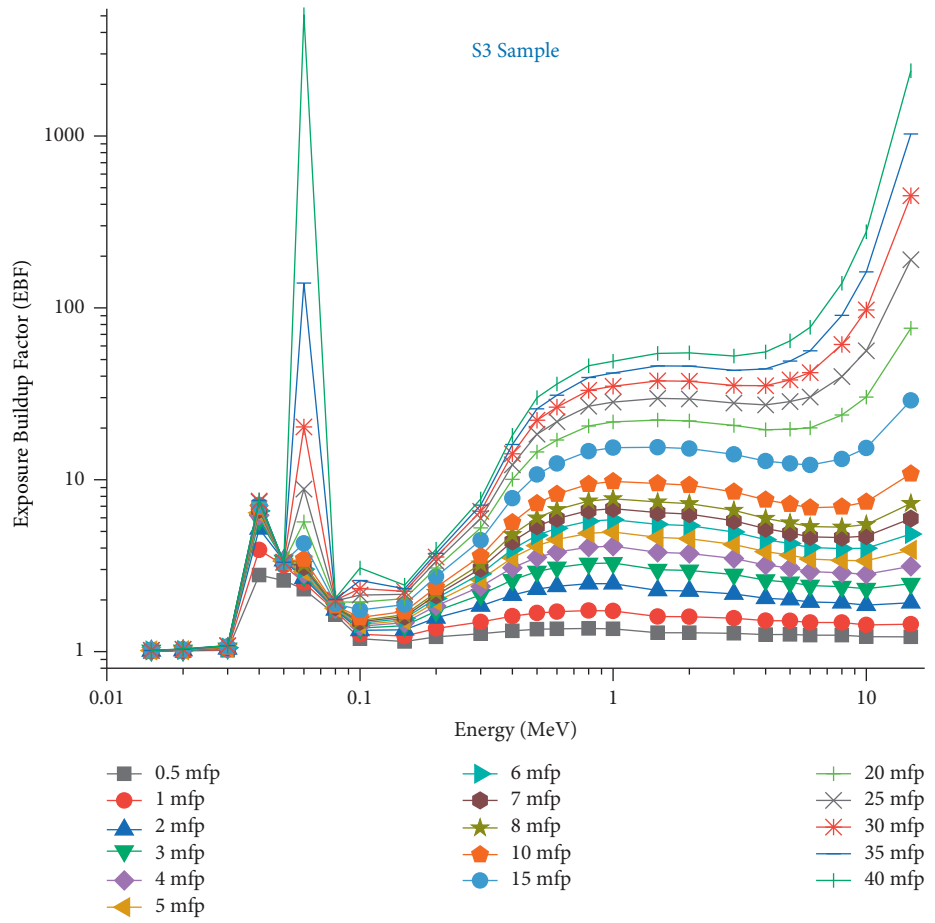


Figure 14: Demonstrates the relationship between the energy and EBF of the S3 sample.

gamma-ray, and hence absorption. The relationship between the effective atomic number ($Z_{eff}$) and the effective electron density ($N_{eff}$) with the incident photon energy differs from previous trends, since they start at a higher value and increase at 0.04 MeV, and then decrease gradually until 1.0 MeV where the trends start increasing again. Both trends exhibit S1 values as the lowest followed by an increase in S2 and S3, giving S3 the highest rank of values (See Figures 8 and 9). Therefore, it can be said that the replacement of 2% moles $Nb_2O_3$ with 1% mole $Ta_2O_5$+ 1% mole $ZrO_2$ caused an increment in the $Z_{eff}$ and $N_{eff}$ values of S1, S2, and S3 glasses. Figures 10–15 demonstrate the studied glasses' exposure build-up factor (EBF) and energy absorption build-up factor (EABF) values as a function of energy (MeV) at different mean free path (i.e., from 0.5 to 40) values. Similar behaviors are reported as a function of photon energy, with a substantial rise in these values at 0.04, 0.06, 0.08, 0.1, and 15 MeV energies, respectively (see Tables 3–5). Variations in the EBF and EABF values are less at smaller penetration depths up to 15 MeV energy, yet they significantly increase with increasing mfp where the energy intensifies up to 15 MeV. The build-up of photons usually occurs at higher mfp values, particularly for thicker materials and a greater diversity of incoming X-rays or gamma rays [53–57]. Our findings clearly indicated that S1 ranks the highest followed by S2 with a slight decrease, and subsequently S3 ranks the lowest. In general, our findings for basic gamma-ray-shielding qualities indicated that the S3 sample exhibits the greatest attenuation among the three glasses investigated. The final assessment step of this research compared the HVL values of the S3 sample, which demonstrated the best performances across all gamma-ray reduction parameters to those of many other glass- and concrete-shielding materials. The compared materials and their codes are listed as follows.

(i) Glass shields: PNCKM5 [58], C25 [59], SCNZ7 [60], Gd10 [61], Gd15 [62].

(ii) Concrete shields: OC, HSC, ILC, BMC, IC, SSC [63].

To begin, all HVL values for the S3 sample were compared to those of other glassy shielding materials whose gamma-ray attenuation characteristics had been previously reported for the same gamma-ray energy range. As seen in Figure 16, the S3 sample's gamma-ray attenuation properties are much greater than those of the glass materials tested. The primary explanation for this condition is the disparity between the heavy element additions in the glass composition and the density increase caused indirectly by this additive. Additionally, the HVL values of the S3 sample were compared to those of many concrete-shielding materials functioning in the same energy range. These concrete materials, including

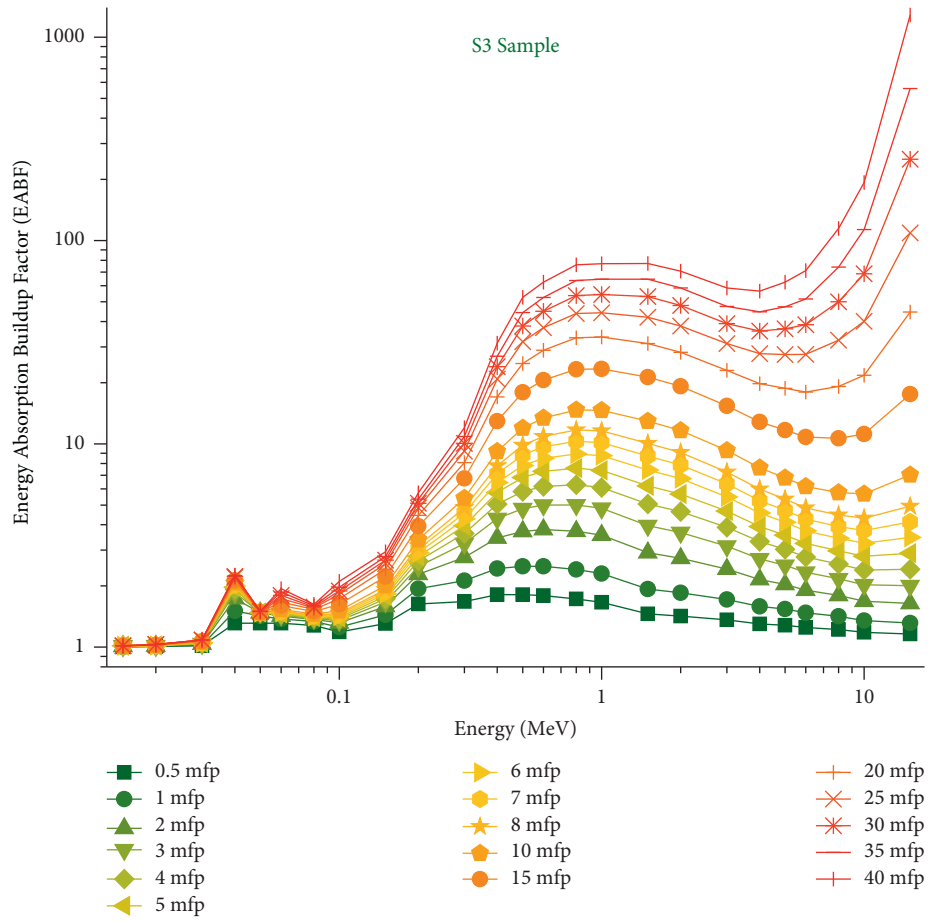


Figure 15: Demonstrates the relationship between the energy and EABF of the S3 sample.

Table 3: (EBF and EABF) G–P fitting coefficients ($b$, $c$, $a$, $X_k$, and $d$) of the S1 sample.

| Energy (MeV) | $Z_{eq}$ | G–P fitting parameters for EBF | | | | | G–P fitting parameters for EABF | | | | |
|---|---|---|---|---|---|---|---|---|---|---|---|
| | | $a$ | $b$ | $c$ | $d$ | $X_k$ | $a$ | $b$ | $c$ | $d$ | $X_k$ |
| 0.015 | 22.62 | −0.249 | 1.006 | 1.049 | 0.234 | 6.358 | −0.242 | 1.006 | 1.043 | 0.225 | 7.785 |
| 0.020 | 26.03 | 0.621 | 1.012 | 0.130 | −0.621 | 11.384 | 0.320 | 1.010 | 0.258 | −0.297 | 18.162 |
| 0.030 | 26.53 | 0.193 | 1.027 | 0.371 | −0.268 | 26.131 | 0.251 | 1.025 | 0.328 | −0.189 | 17.470 |
| 0.040 | 42.71 | 0.089 | 3.906 | 0.409 | −0.041 | 23.655 | 0.105 | 1.506 | 0.411 | −0.043 | 22.264 |
| 0.050 | 43.19 | −0.221 | 3.170 | 0.111 | 0.009 | 12.737 | −0.084 | 1.424 | 0.123 | 0.064 | 9.645 |
| 0.060 | 43.54 | 0.870 | 2.519 | 0.051 | −0.129 | 14.938 | 0.618 | 1.377 | 0.071 | −0.141 | 16.201 |
| 0.080 | 43.96 | 0.779 | 1.699 | 0.029 | −0.229 | 14.675 | 0.615 | 1.324 | 0.069 | −0.228 | 14.092 |
| 0.100 | 44.24 | 0.409 | 1.229 | 0.227 | −0.205 | 13.762 | 0.427 | 1.237 | 0.198 | −0.225 | 13.677 |
| 0.150 | 44.65 | 0.211 | 1.233 | 0.432 | −0.113 | 14.255 | 0.337 | 1.444 | 0.272 | −0.186 | 14.016 |
| 0.200 | 44.88 | 0.172 | 1.393 | 0.509 | −0.096 | 14.415 | 0.321 | 2.031 | 0.298 | −0.196 | 13.988 |
| 0.300 | 45.14 | 0.091 | 1.513 | 0.697 | −0.046 | 14.383 | 0.178 | 2.192 | 0.516 | −0.105 | 13.961 |
| 0.400 | 45.28 | 0.050 | 1.633 | 0.847 | −0.037 | 14.163 | 0.126 | 2.498 | 0.661 | −0.096 | 13.893 |
| 0.500 | 45.36 | 0.028 | 1.701 | 0.931 | −0.029 | 14.211 | 0.085 | 2.549 | 0.775 | −0.073 | 13.887 |
| 0.600 | 45.41 | 0.013 | 1.728 | 0.984 | −0.021 | 13.976 | 0.063 | 2.537 | 0.840 | −0.061 | 13.747 |
| 0.800 | 45.47 | −0.001 | 1.749 | 1.039 | −0.015 | 14.052 | 0.038 | 2.433 | 0.920 | −0.047 | 13.646 |
| 1.000 | 45.49 | −0.007 | 1.739 | 1.063 | −0.013 | 13.430 | 0.025 | 2.319 | 0.961 | −0.038 | 13.527 |
| 1.500 | 44.50 | −0.027 | 1.606 | 1.148 | −0.001 | 9.504 | −0.006 | 1.933 | 1.074 | −0.018 | 13.533 |
| 2.000 | 41.99 | −0.021 | 1.601 | 1.127 | −0.005 | 12.618 | 0.002 | 1.850 | 1.048 | −0.024 | 13.068 |
| 3.000 | 39.09 | −0.001 | 1.569 | 1.064 | −0.026 | 12.718 | 0.028 | 1.711 | 0.972 | −0.049 | 13.028 |
| 4.000 | 38.00 | 0.014 | 1.516 | 1.023 | −0.038 | 13.241 | 0.042 | 1.584 | 0.936 | −0.062 | 13.671 |
| 5.000 | 37.42 | 0.036 | 1.507 | 0.963 | −0.058 | 13.487 | 0.064 | 1.533 | 0.883 | −0.082 | 13.895 |
| 6.000 | 37.01 | 0.045 | 1.473 | 0.946 | −0.065 | 13.619 | 0.071 | 1.469 | 0.870 | −0.088 | 14.102 |
| 8.000 | 36.58 | 0.064 | 1.465 | 0.909 | −0.082 | 13.907 | 0.083 | 1.409 | 0.854 | −0.097 | 14.200 |
| 10.000 | 36.34 | 0.052 | 1.419 | 0.964 | −0.070 | 14.093 | 0.069 | 1.340 | 0.909 | −0.083 | 14.342 |
| 15.000 | 36.25 | 0.042 | 1.421 | 1.059 | −0.062 | 14.287 | 0.061 | 1.301 | 0.989 | −0.076 | 14.491 |

Table 4: (EBF and EABF) G–P fitting coefficients ($b$, $c$, $a$, $X_k$, and $d$) of the S2 sample.

| Energy (MeV) | $Z_{eq}$ | G–P fitting parameters for EBF | | | | | G–P fitting parameters for EABF | | | | |
|---|---|---|---|---|---|---|---|---|---|---|---|
| | | $a$ | $b$ | $c$ | $d$ | $X_k$ | $a$ | $b$ | $c$ | $d$ | $X_k$ |
| 0.015 | 23.17 | −0.302 | 1.005 | 1.138 | 0.254 | 6.228 | −0.296 | 1.005 | 1.133 | 0.247 | 7.408 |
| 0.020 | 26.18 | 0.629 | 1.012 | 0.128 | −0.644 | 11.352 | 0.327 | 1.010 | 0.256 | −0.309 | 17.867 |
| 0.030 | 26.67 | 0.193 | 1.026 | 0.371 | −0.255 | 25.314 | 0.251 | 1.025 | 0.330 | −0.188 | 17.111 |
| 0.040 | 42.70 | 0.089 | 3.906 | 0.407 | −0.041 | 23.649 | 0.105 | 1.505 | 0.409 | −0.043 | 22.283 |
| 0.050 | 43.17 | −0.223 | 3.169 | 0.110 | 0.010 | 12.724 | −0.085 | 1.423 | 0.121 | 0.065 | 9.623 |
| 0.060 | 43.52 | 0.873 | 2.517 | 0.051 | −0.129 | 14.973 | 0.621 | 1.376 | 0.071 | −0.141 | 16.183 |
| 0.080 | 44.88 | 0.784 | 1.717 | 0.027 | −0.217 | 14.799 | 0.634 | 1.335 | 0.063 | −0.228 | 14.116 |
| 0.100 | 45.19 | 0.457 | 1.258 | 0.198 | −0.225 | 13.767 | 0.467 | 1.254 | 0.176 | −0.248 | 13.631 |
| 0.150 | 45.66 | 0.224 | 1.230 | 0.411 | −0.121 | 14.195 | 0.355 | 1.443 | 0.254 | −0.196 | 13.985 |
| 0.200 | 45.91 | 0.172 | 1.365 | 0.507 | −0.095 | 14.459 | 0.322 | 1.945 | 0.295 | −0.195 | 13.974 |
| 0.300 | 46.22 | 0.094 | 1.488 | 0.686 | −0.047 | 14.347 | 0.184 | 2.128 | 0.502 | −0.108 | 13.928 |
| 0.400 | 46.39 | 0.053 | 1.608 | 0.832 | −0.038 | 14.157 | 0.132 | 2.440 | 0.643 | −0.099 | 13.887 |
| 0.500 | 46.49 | 0.032 | 1.678 | 0.916 | −0.031 | 14.173 | 0.090 | 2.502 | 0.758 | −0.076 | 13.883 |
| 0.600 | 46.57 | 0.016 | 1.707 | 0.971 | −0.022 | 13.987 | 0.068 | 2.500 | 0.823 | −0.064 | 13.742 |
| 0.800 | 46.64 | 0.002 | 1.731 | 1.029 | −0.016 | 14.062 | 0.042 | 2.410 | 0.905 | −0.049 | 13.642 |
| 1.000 | 46.66 | −0.005 | 1.724 | 1.054 | −0.014 | 13.430 | 0.028 | 2.303 | 0.948 | −0.040 | 13.520 |
| 1.500 | 45.66 | −0.026 | 1.598 | 1.142 | −0.002 | 10.567 | −0.004 | 1.929 | 1.065 | −0.019 | 13.561 |
| 2.000 | 43.09 | −0.020 | 1.594 | 1.124 | −0.006 | 12.691 | 0.004 | 1.850 | 1.040 | −0.026 | 13.077 |
| 3.000 | 39.98 | −0.001 | 1.565 | 1.064 | −0.026 | 12.756 | 0.030 | 1.714 | 0.967 | −0.052 | 13.085 |
| 4.000 | 38.79 | 0.014 | 1.514 | 1.023 | −0.039 | 13.265 | 0.045 | 1.588 | 0.930 | −0.065 | 13.640 |
| 5.000 | 38.17 | 0.038 | 1.509 | 0.959 | −0.060 | 13.505 | 0.067 | 1.539 | 0.874 | −0.086 | 13.876 |
| 6.000 | 37.75 | 0.047 | 1.477 | 0.942 | −0.067 | 13.650 | 0.075 | 1.476 | 0.861 | −0.092 | 14.087 |
| 8.000 | 37.26 | 0.066 | 1.473 | 0.904 | −0.084 | 13.940 | 0.087 | 1.418 | 0.846 | −0.100 | 14.212 |
| 10.000 | 37.02 | 0.053 | 1.429 | 0.964 | −0.071 | 14.108 | 0.071 | 1.349 | 0.905 | −0.085 | 14.343 |
| 15.000 | 36.90 | 0.041 | 1.439 | 1.066 | −0.061 | 14.272 | 0.061 | 1.314 | 0.992 | −0.077 | 14.465 |

Table 5: (EBF and EABF) G–P fitting coefficients ($b$, $c$, $a$, $X_k$, and $d$) of the S3 sample.

| Energy (MeV) | $Z_{eq}$ | G–P fitting parameters for EBF | | | | | G–P fitting parameters for EABF | | | | |
|---|---|---|---|---|---|---|---|---|---|---|---|
| | | $a$ | $b$ | $c$ | $d$ | $X_k$ | $a$ | $b$ | $c$ | $d$ | $X_k$ |
| 0.015 | 23.21 | −0.305 | 1.005 | 1.144 | 0.256 | 6.218 | −0.300 | 1.005 | 1.139 | 0.248 | 7.381 |
| 0.020 | 26.08 | 0.624 | 1.012 | 0.129 | −0.629 | 11.372 | 0.323 | 1.010 | 0.257 | −0.301 | 18.059 |
| 0.030 | 26.56 | 0.193 | 1.026 | 0.371 | −0.265 | 25.934 | 0.251 | 1.025 | 0.328 | −0.189 | 17.383 |
| 0.040 | 42.76 | 0.089 | 3.903 | 0.415 | −0.042 | 23.675 | 0.105 | 1.507 | 0.417 | −0.043 | 22.196 |
| 0.050 | 43.24 | −0.217 | 3.172 | 0.114 | 0.007 | 12.768 | −0.082 | 1.426 | 0.125 | 0.062 | 9.699 |
| 0.060 | 43.58 | 0.863 | 2.522 | 0.053 | −0.128 | 14.864 | 0.613 | 1.378 | 0.073 | −0.139 | 16.238 |
| 0.080 | 44.95 | 0.784 | 1.718 | 0.027 | −0.216 | 14.809 | 0.635 | 1.336 | 0.063 | −0.228 | 14.118 |
| 0.100 | 45.26 | 0.461 | 1.260 | 0.195 | −0.227 | 13.767 | 0.470 | 1.255 | 0.174 | −0.250 | 13.627 |
| 0.150 | 45.73 | 0.225 | 1.230 | 0.410 | −0.122 | 14.191 | 0.356 | 1.443 | 0.253 | −0.197 | 13.983 |
| 0.200 | 45.99 | 0.172 | 1.363 | 0.507 | −0.095 | 14.462 | 0.322 | 1.939 | 0.295 | −0.195 | 13.973 |
| 0.300 | 46.29 | 0.095 | 1.486 | 0.685 | −0.047 | 14.345 | 0.185 | 2.124 | 0.502 | −0.108 | 13.926 |
| 0.400 | 46.46 | 0.054 | 1.607 | 0.831 | −0.039 | 14.157 | 0.133 | 2.436 | 0.642 | −0.099 | 13.887 |
| 0.500 | 46.56 | 0.032 | 1.677 | 0.915 | −0.031 | 14.170 | 0.091 | 2.500 | 0.757 | −0.077 | 13.882 |
| 0.600 | 46.64 | 0.016 | 1.705 | 0.971 | −0.022 | 13.988 | 0.068 | 2.498 | 0.822 | −0.064 | 13.742 |
| 0.800 | 46.71 | 0.002 | 1.730 | 1.028 | −0.016 | 14.063 | 0.042 | 2.409 | 0.904 | −0.049 | 13.642 |
| 1.000 | 46.74 | −0.004 | 1.723 | 1.053 | −0.014 | 13.430 | 0.029 | 2.302 | 0.948 | −0.040 | 13.519 |
| 1.500 | 45.74 | −0.026 | 1.598 | 1.142 | −0.002 | 10.636 | −0.004 | 1.929 | 1.065 | −0.019 | 13.563 |
| 2.000 | 43.17 | −0.020 | 1.594 | 1.124 | −0.006 | 12.696 | 0.005 | 1.850 | 1.039 | −0.027 | 13.078 |
| 3.000 | 40.06 | −0.001 | 1.565 | 1.064 | −0.027 | 12.760 | 0.030 | 1.714 | 0.967 | −0.052 | 13.090 |
| 4.000 | 38.87 | 0.015 | 1.514 | 1.023 | −0.039 | 13.268 | 0.045 | 1.588 | 0.929 | −0.065 | 13.637 |
| 5.000 | 38.24 | 0.038 | 1.509 | 0.959 | −0.060 | 13.507 | 0.068 | 1.540 | 0.873 | −0.086 | 13.874 |
| 6.000 | 37.83 | 0.047 | 1.477 | 0.942 | −0.068 | 13.653 | 0.075 | 1.476 | 0.860 | −0.092 | 14.085 |
| 8.000 | 37.34 | 0.067 | 1.474 | 0.904 | −0.085 | 13.944 | 0.087 | 1.419 | 0.845 | −0.101 | 14.214 |
| 10.000 | 37.10 | 0.053 | 1.431 | 0.964 | −0.071 | 14.110 | 0.072 | 1.350 | 0.905 | −0.085 | 14.343 |
| 15.000 | 36.97 | 0.041 | 1.442 | 1.067 | −0.061 | 14.270 | 0.061 | 1.315 | 0.993 | −0.077 | 14.462 |

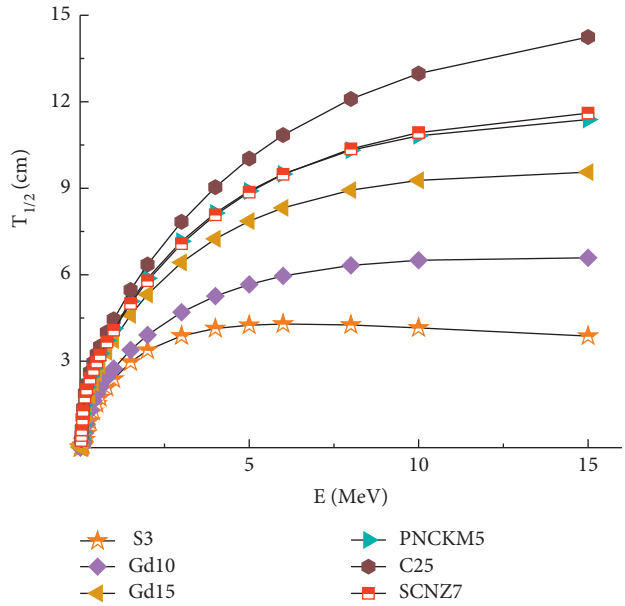


Figure 16: Comparison of the HVL values with different types of glasses.

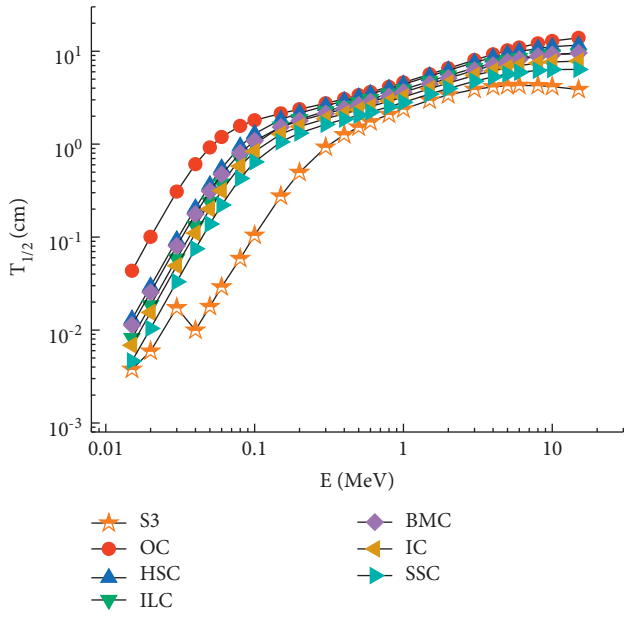


Figure 17: Comparison of the HVL values with different types of concrete shields.

ordinary concrete (OC), were determined as other concretes such as HSC, BMC, ILC, SSC, and IC with some additives that increase the shielding properties. Comparison of the critical HVL values of the S3 sample with these concrete types is shown in Figure 17. As can be seen, especially at low energy levels, the HVL values of the S3 sample are much lower than those compared with the concrete samples. On the other hand, this advantageous situation in HVL values was also seen in all energy values studied. Although concrete is still the most effective and preferred shielding material for medical and industrial radiation fields, there are also disadvantages of this material. For this reason, the production and development of superior glassy shields such as the S3 sample, which can be an alternative to concrete and especially overcome the critical disadvantages of concrete, will make important contributions to the material literature, as well as enable the reshaping of the shielding materials recommended in radiation protection procedures.

## 4. Conclusion

The use of glass and glass-based materials for shielding in radiation fields has increased visibly in recent years. Some of the most main causes for this expansion are that glass constructions are incredibly adaptable to development and may be manufactured with a variety of components and their combinations in varying proportions. On the other hand, it is extremely important to understand the monotonic effect of certain types of additive ratios that increase or decrease in the glass composition during the production of glass series. The aim of this study was to examine the radiation attenuation difference occurring in the studied borotellurite glass structures according to the varying additive ratio and to discuss the rationale behind the positive change in the shielding ability. The glass samples that have been investigated in the current investigation were previously assessed in terms of their nonlinear refractive index. The initial outcome results indicate that while the modifier oxides have an effect on the structural units and polarizability of the glass, they are insufficient to alter the behavior of the nonlinear refractive index spectra, with the glass matrix being the primary source of optical nonlinearity in the system under study. As with prior results for other characteristics, our findings clearly demonstrate that although some behavioral changes occurred in the shielding qualities, modest improvements occurred in the attenuation properties depending on the modifier variation and its magnitude. However, the replacement of 2% moles of $Nb_2O_5$ with 1% mole of $Ta_2O_5$ and 1% mole of $ZrO_2$ provided significant improvements in both glass density and attenuation properties against gamma rays. While concrete remains the most efficient and favored shielding material in medical and industrial radiation sectors, it does have certain drawbacks. As a result, the production and development of superior glassy shields, such as the S3 sample that can be used in place of concrete and specifically overcome its critical disadvantages, will contribute significantly to the material literature, and enable the reshaping of shielding materials recommended in radiation protection procedures. As a consequence of this investigation, it can be concluded that the indicated type of additive to be added to borotellurite glasses will provide some advantages, particularly when used in radiation fields, by increasing the shielding qualities moderately. Additionally, supplementary material characterizations of the relevant glass types are recommended, and it would be beneficial to extend this follow-up research and provide additional data to the literature in order to fully understand and apply the relevant glass type's terms of use.

## Data Availability

The data presented in this study are available on request from the corresponding author.

## Conflicts of Interest

The authors declare that they have no conflicts of interest.

## Acknowledgments

This work was performed under Princess Nourah Bint Abdulrahman University Researchers Supporting Project Number (PNURSP2022R149), Princess Nourah Bint Abdulrahman University, Riyadh, Saudi Arabia. Therefore, the authors express their sincere gratitude to Princess Nourah Bint Abdulrahman University. The work of Antoaneta Ene and the APC were supported by Dunarea de Jos University of Galati, Romania. The researcher (H.M.H.Z) is supported by a scholarship under the Joint (Executive Program between Egypt and Russia).

## References

[1] D. Adliene, B. Griciene, K. Skovorodko, J. Laurikaitiene, and J. Puiso, "Occupational radiation exposure of health professionals and cancer risk assessment for lithuanian nuclear medicine workers," *Environmental Research*, vol. 183, Article ID 109144, 2020.

[2] A. Fawazi, A. El-Sayes, A. El-Latif, and M. El-Desoky, "Borate glass with lead and nickel oxides for radiation attenuation," *Abhath Al-Yarmouk*, vol. 15, no. 2, pp. 195–205, 2006.

[3] K. J. Singh, N. Singh, R. S. Kaundal, and K. Singh, "Gamma-ray shielding and structural properties of PbO-$SiO_2$ glasses," *Nuclear Instruments and Methods in Physics Research Section B: Beam Interactions with Materials and Atoms*, vol. 266, no. 6, pp. 944–948, 2008.

[4] I. Mustafa, H. Kamari, W. Yusoff, S. Aziz, and A. Rahman, "Structural and optical properties of lead-boro-tellurrite glasses induced by gamma-ray," *International Journal of Molecular Sciences*, vol. 14, no. 2, pp. 3201–3214, 2013.

[5] J. Kaewkhao and P. Limsuwan, "Mass attenuation coefficients and effective atomic numbers in phosphate glass containing bi2o3, pbo and bao at 662 kev," *Nuclear Instruments and Methods in Physics Research Section A: Accelerators, Spectrometers, Detectors and Associated Equipment*, vol. 619, no. 1–3, pp. 295–297, 2010.

[6] P. Limkitjaroenporn, J. Kaewkhao, P. Limsuwan, and W. Chewpraditkul, "Physical, optical, structural and gamma-ray shielding properties of lead sodium borate glasses," *Journal of Physics and Chemistry of Solids*, vol. 72, no. 4, pp. 245–251, 2011.

[7] V. P. Singh and N. M. Badiger, "Shielding efficiency of lead borate and nickel borate glasses for gamma rays and neutrons," *Glass Physics and Chemistry*, vol. 41, no. 3, pp. 276–283, 2015.

[8] A. Kumar, M. I. Sayyed, M. Dong, and X. Xue, "Effect of PbO on the shielding behavior of ZnO-P2O5 glass system using Monte Carlo simulation," *Journal of Non-crystalline Solids*, vol. 481, pp. 604–607, 2018.

[9] Y. Al-Hadeethi and M. I. Sayyed, "The influence of pbo on the radiation attenuation features of tellurite glass," *Ceramics International*, vol. 45, no. 18, pp. 24230–24235, 2019.

[10] R. A. El-Mallawany, *Tellurite Glasses Handbook: Physical Properties and Data*, CRC Press, Florida, FL, USA, 2016.

[11] D. Dutta and A. Ghosh, "Dynamics of ag+ ions in binary tellurite glasses," *Physical Review B: Condensed Matter*, vol. 72, no. 2, Article ID 024201, 2005.

[12] N. Elkhoshkhany, R. Abbas, R. El-Mallawany, and k. S. H. Humoud Sharba, "Thermal properties of quaternary TeO2-ZnO-Nb2O5-Gd2O3 glasses," *Ceramics International*, vol. 40, no. 8, pp. 11985–11994, 2014.

[13] N. Elkhoshkhany, R. Abbas, R. El-Mallawany, and A. J. Fraih, "Optical Properties of quaternary TeO2-ZnO-Nb2O5-Gd2O3 glasses," *Ceramics International*, vol. 40, no. 9, pp. 14477–14481, 2014.

[14] N. Elkhoshkhany, R. Abbas, M. S. Gaafar, and R. El-Mallawany, "Elastic properties of quaternaryTeO2-ZnO-Nb2O5-Gd2O3 glasses," *Ceramics International*, vol. 41, no. 8, pp. 9862–9866, 2015.

[15] N. Elkhoshkhany and R. El-Mallawany, "Optical and kinetics parameters of lithium boro-tellurite glasses," *Ceramics International*, vol. 41, no. 3, pp. 3561–3567, 2015.

[16] R. El-Mallawany, M. Sidkey, A. Khafagy, and H. Afifi, "Ultrasonic attenuation of tellurite glasses," *Materials Chemistry and Physics*, vol. 37, no. 2, pp. 197–200, 1994.

[17] J. Li, Z. Sun, X. Zhu et al., "Optical bistability for ZnO-Nb2O5-TeO2 glasses," *Optical Materials*, vol. 25, no. 4, pp. 401–405, 2004.

[18] T. Hayakawa, M. Hayakawa, M. Nogami, and P. Thomas, "Nonlinear optical properties and glass structure for MO-Nb2O5-TeO2 (M=Zn, Mg, Ca, Sr, Ba) glasses," *Optical Materials*, vol. 32, no. 3, pp. 448–455, 2010.

[19] B. Samanta, D. Dutta, and S. Ghosh, "Synthesis and different optical properties of Gd 2 O 3 doped sodium zinc tellurite glasses," *Physica B: Condensed Matter*, vol. 515, pp. 82–88, 2017.

[20] D. K. Gaikwad, M. I. Sayyed, S. S. Obaid, S. A. M. Issa, and P. P. Pawar, "Gamma ray shielding properties of teo2-znf2-as2o3-sm2o3 glasses," *Journal of Alloys and Compounds*, vol. 765, pp. 451–458, 2018.

[21] M. I. Sayyed, H. O. Tekin, and O. Agar, "Gamma photon and neutron attenuation properties of MgO-BaO-B2O3-TeO2-Cr2O3 glasses: the role of TeO2," *Radiation Physics and Chemistry*, vol. 163, pp. 58–66, 2019.

[22] A. E. Ersundu, M. Büyükyıldız, M. Çelikbilek Ersundu, E. Şakar, and M. Kurudirek, "The heavy metal oxide glasses within the WO 3 -MoO 3 -TeO 2 system to investigate the shielding properties of radiation applications," *Progress in Nuclear Energy*, vol. 104, pp. 280–287, 2018.

[23] M. I. Sayyed and R. El-Mallawany, "Shielding properties of (100-x)TeO 2 -(x)MoO 3 glasses," *Materials Chemistry and Physics*, vol. 201, pp. 50–56, 2017.

[24] Y. Al-Hadeethi, M. Sayyed, and S. Tijani, "Gamma radiation attenuation properties of tellurite glasses: a comparative study," *Nuclear Engineering and Technology*, vol. 51, no. 8, pp. 2005–2012, 2019.

[25] M. I. Sayyed, M. G. Dong, H. O. Tekin, G. Lakshminarayana, and M. A. Mahdi, "Comparative investigations of gamma and neutron radiation shielding parameters for different borate and tellurite glass systems using winxcom program and mcnpx code," *Materials Chemistry and Physics*, vol. 215, pp. 183–202, 2018.

[26] M. K. Halimah, A. Azuraida, M. Ishak, and L. Hasnimulyati, "Influence of bismuth oxide on gamma radiation shielding properties of boro-tellurite glass," *Journal of Non-crystalline Solids*, vol. 512, pp. 140–147, 2019.

[27] Y. Al-Hadeethi and M. I. Sayyed, "A comprehensive study on the effect of TeO2 on the radiation shielding properties of TeO2-B2O3-Bi2O3-LiF-SrCl2 glass system using Phy-X/PSD software," *Ceramics International*, vol. 46, no. 5, pp. 6136–6140, 2020.

[28] M. I. Sayyed, Y. Al-Hadeethi, M. M. AlShammari, M. Ahmed, S. H. Al-Heniti, and Y. S. Rammah, "Physical, optical and gamma radiation shielding competence of newly boro-tellurite based glasses: TeO2-B2O3-ZnO-Li2O3-Bi2O3," *Ceramics International*, vol. 47, no. 1, pp. 611–618, 2021.

[29] M. I. Sayyed, A. A. Ali, H. O. Tekin, and Y. S. Rammah, "Investigation of gamma-ray shielding properties of bismuth borotellurite glasses using MCNPX code and XCOM program," *Applied Physics A*, vol. 125, no. 6, p. 445, 2019.

[30] H. Desirena, A. Schülzgen, S. Sabet, G. Ramos-Ortiz, E. de la Rosa, and N. Peyghambarian, "Effect of alkali metal oxides R2O (R=Li, Na, K, Rb and Cs) and network intermediate MO (M=Zn, Mg, Ba and Pb) in tellurite glasses," *Optical Materials*, vol. 31, no. 6, pp. 784–789, 2009.

[31] G. Kilic, "Role of Nd3+ ions in TeO2-V2O5-(B2O3/Nd2O3) glasses: structural, optical, and thermal characterization," *Journal of Materials Science: Materials in Electronics*, vol. 31, no. 15, pp. 12892–12902, 2020.

[32] A. G. Kalampounias, G. N. Papatheodorou, and S. N. Yannopoulos, "A temperature dependence Raman study of the 0.1Nb2O5-0.9TeO2 glass-forming system," *Journal of Physics and Chemistry of Solids*, vol. 67, no. 4, pp. 725–731, 2006.

[33] M. R. Zaki, D. Hamani, M. Dutreilh-Colas et al., "Structural investigation of new tellurite glasses belonging to the TeO2-NbO2.5-WO3 system, and a study of their linear and nonlinear optical properties," *Journal of Non-crystalline Solids*, vol. 512, pp. 161–173, 2019.

[34] S. A. M. Issa, M. Rashad, H. M. H. Zakaly, H. O. Tekin, and A. S. Abouhaswa, "Nb2O5-Li2O-Bi2O3-B2O3 novel glassy system: evaluation of optical, mechanical, and gamma shielding parameters," *Journal of Materials Science: Materials in Electronics*, vol. 31, pp. 22039–22056, 2020.

[35] G. Guery, A. Fargues, T. Cardinal et al., "Impact of tellurite-based glass structure on Raman gain," *Chemical Physics Letters*, vol. 554, pp. 123–127, 2012.

[36] S.-H. Kim and T. Yoko, "Nonlinear optical properties of TeO2-based glasses: MOx-TeO2 (M = Sc, Ti, V, Nb, Mo, Ta, and W) binary glasses," *Journal of the American Ceramic Society*, vol. 78, no. 4, pp. 1061–1065, 1995.

[37] R. Karell, M. Chromčíková, and M. Liška, "Properties of selected zirconia containing silicate glasses III," *J. Ceram.*vol. 52, pp. 102–108, 2008.

[38] S. Khan, G. Kaur, and K. Singh, "Effect of ZrO2 on dielectric, optical and structural properties of yttrium calcium borosilicate glasses," *Ceramics International*, vol. 43, no. 1, pp. 722–727, 2017.

[39] K. V. Krishnaiah, P. Venkatalakshmamma, C. Basavapoornima et al., "Er3+-doped tellurite glasses for enhancing a solar cell photocurrent through photon upconversion upon 1500 nm excitation," *Materials Chemistry and Physics*, vol. 199, pp. 67–72, 2017.

[40] A. G. Pelosi, S. N. C. Santos, J. Dipold et al., "Effects of modifier oxides in the nonlinear refractive index of niobium-borotellurite glasses," *Journal of Alloys and Compounds*, vol. 878, Article ID 160382, 2021.

[41] R. S. I. C. C. Collection, "MCNPX User's Manual Version 2.4.0. Monte Carlo N-Particle Transport Code System for Multiple and High Energy Applications," 2002, http://www.nea.fr/abs/html/ccc-0715.html.

[42] E. Sakar, Ö. F. Özpolat, B. Alım, M. Sayyed, and M. Kurudirek, "Phy-X/PSD: development of a user friendly online software for calculation of parameters relevant to radiation shielding and dosimetry," *Radiation Physics and Chemistry*, vol. 166, Article ID 108496, 2020.

[43] Y. Al-Hadeethi, M. I. Sayyed, J. Kaewkhao et al., "Physical, structural, optical, and radiation shielding properties of

B2O3-Gd2O3-Y2O3 glass system," *Applied Physics A*, vol. 125, no. 12, p. 852, 2019.

[44] M. I. Sayyed, H. O. Tekin, O. Kılıcoglu, O. Agar, and M. H. M. Zaid, "Shielding features of concrete types containing sepiolite mineral: comprehensive study on experimental, XCOM and MCNPX results," *Results in Physics*, vol. 11, pp. 40–45, 2018.

[45] M. Almatari, O. Agar, E. E. Altunsoy, O. Kilicoglu, M. I. Sayyed, and H. O. Tekin, "Photon and neutron shielding characteristics of samarium doped lead alumino borate glasses containing barium, lithium and zinc oxides determined at medical diagnostic energies," *Results in Physics*, vol. 12, pp. 2123–2128, 2019.

[46] G. Lakshminarayana, A. Kumar, O. Tekin et al., "Binary B2O3-Bi2O3 glasses: scrutinization of directly and indirectly ionizing radiations shielding abilities," *Journal of Materials Research and Technology*, vol. 9, no. 6, pp. 14549–14567, 2020.

[47] G. Lakshminarayana, A. Kumar, H. O. Tekin et al., "In-depth survey of nuclear radiation attenuation efficacies for high density bismuth lead borate glass system," *Results in Physics*, vol. 23, Article ID 104030, 2021.

[48] G. Kilic, E. Ilik, S. A. M. Issa et al., "Ytterbium (III) oxide reinforced novel TeO2-B2O3-V2O5 glass system: synthesis and optical, structural, physical and thermal properties," *Ceramics International*, vol. 47, no. 13, pp. 18517–18531, 2021.

[49] G. Lakshminarayana, Y. Elmahroug, A. Kumar et al., "Detailed inspection of $\gamma$-ray, fast and thermal neutrons shielding competence of calcium oxide or strontium oxide comprising bismuth borate glasses," *Materials*, vol. 14, no. 9, p. 2265, 2021.

[50] G. Lakshminarayana, A. Kumar, H. O. Tekin et al., "Probing of nuclear radiation attenuation and mechanical features for lithium bismuth borate glasses with improving Bi2O3 content for B2O3+Li2O amounts," *Results in Physics Available online*, vol. 25, 2021.

[51] G. ALMisned, H. O. Tekin, E. Kavaz et al., "Antoaneta ene. Gamma, fast neutron, proton, and alpha shielding properties of borate glasses: a closer look on lead (II) oxide and bismuth (III) oxide reinforcement," *Applied Sciences*, vol. 11, p. 15, 2021.

[52] G. ALMisned, H. O. Tekin, S. A. M. Issa et al., "Novel HMO-glasses with Sb2O3 and TeO2 for nuclear radiation shielding purposes: a comparative analysis with traditional and novel shields," *Materials*, vol. 14, no. 15, p. 4330, 2021.

[53] G. Lakshminarayana, S. A. M. Issa, Y. B. Saddeek et al., "Analysis of physical and mechanical traits and nuclear radiation transmission aspects of Gallium(III) trioxide constituting Bi2O3-B2O3 glasses," *Results in Physics*, vol. 30, Article ID 104899, 2021.

[54] G. ALMisned, H. M. H. Zakaly, S. A. M. Issa et al., "Gamma-ray protection properties of bismuth-silicate glasses against some diagnostic nuclear medicine radioisotopes: a comprehensive study," *Materials*, vol. 14, no. 21, p. 6668, 2021.

[55] H. M. H. Zakaly, M. Rashad, H. O. Tekin, H. A. Saudi, S. A. M. Issa, and A. M. A. Henaish, "Synthesis, optical, structural and physical properties of newly developed dolomite reinforced borate glasses for nuclear radiation shielding utilizations: an experimental and simulation study," *Optical Materials*, vol. 114, Article ID 110942, 2021.

[56] G. Lakshminarayana, A. Kumar, H. O. Tekin et al., "Illustration of distinct nuclear radiation transmission factors combined with physical and elastic characteristics of barium boro-bismuthate glasses," *Results in Physics*, vol. 31, Article ID 105067, 2021.

[57] H. M. H. Zakaly, H. A. Saudi, S. A. M. Issa et al., "Alteration of optical, structural, mechanical durability and nuclear radiation attenuation properties of barium borosilicate glasses through BaO reinforcement: experimental and numerical analyses," *Ceramics International*, vol. 47, no. 4, pp. 5587–5596, 2021.

[58] A. Alalawi, M. S. Al-Buriahi, and Y. S. Rammah, "Radiation shielding properties of PNCKM bioactive glasses at nuclear medicine energies," *Ceramics International*, vol. 46, no. 10, pp. 15027–15033, 2020.

[59] G. Susoy, E. E. A. Guclu, O. Kilicoglu et al., "The impact of Cr2O3 additive on nuclear radiation shielding properties of LiF-SrO-B2O3 glass system," *Materials Chemistry and Physics*, vol. 242, Article ID 122481, 2020.

[60] H. Akyildirim, E. Kavaz, F. I. El-Agawany, E. Yousef, and Y. S. Rammah, "Radiation shielding features of zirconolite silicate glasses using XCOM and FLUKA simulation code," *Journal of Non-crystalline Solids*, vol. 545, Article ID 120245, 2020.

[61] Y. Al-Hadeethi, M. I. Sayyed, B. M. Raffah, E. Bekyarova, and Y. S. Rammah, "Optical properties and radiation shielding features of Er3+ ions doped B2O3–SiO2–Gd2O3–CaO glasses," *Ceramics International*, vol. 47, p. 3, 2021.

[62] F. Zaman, G. Rooh, N. Srisittipokakun et al., "Scintillation and luminescence characteristics of Ce3+doped in Li2O-Gd2O3-BaO-B2O3 scintillating glasses," *Radiation Physics and Chemistry*, vol. 130, pp. 158–163, 2017.

[63] I. I. Bashter, "Calculation of radiation attenuation coefficients for shielding concretes," *Annals of Nuclear Energy*, vol. 24, no. 17, pp. 1389–1401, 1997.